ORIGINAL ARTICLE

S100-A10, thioredoxin, and S100-A6 as biomarkers of papillary thyroid carcinoma with lymph node metastasis identified by MALDI Imaging

**Martin Nipp · Mareike Elsner · Benjamin Balluff · Stephan Meding ·
Hakan Sarioglu · Marius Ueffing · Sandra Rauser · Kristian Unger · Heinz Höfler ·
Axel Walch · Horst Zitzelsberger**

Abstract In papillary thyroid carcinoma (PTC), metastasis is a feature of an aggressive tumor phenotype. To identify protein biomarkers that distinguish patients with an aggressive tumor behavior, proteomic signatures in metastatic and non-metastatic tumors were investigated comparatively. In particular, matrix-assisted laser desorption/ionization (MALDI) imaging mass spectrometry (IMS) was used to analyze primary tumor samples. We investigated a tumor cohort of PTC ($n=118$) that were matched for age, tumor stage, and gender. Proteomic screening by MALDI-IMS was performed for a discovery set ($n=29$). Proteins related to the discriminating mass peaks were identified by 1D-gel electrophoresis followed by mass spectrometry. The candidate proteins were subsequently validated by immunohistochemistry (IHC) using a tissue microarray for an independent PTC validation set ($n=89$). In this study, we found 36 mass-to-charge-ratio (m/z) species that specifically distinguished metastatic from non-metastatic tumors, among which m/z 11,608 was identified as thioredoxin, m/z 11,184 as S100-A10, and m/z 10,094 as S100-A6. Furthermore, using IHC on the validation set, we showed that the overexpression of these three proteins was highly associated with lymph node metastasis in PTC ($p<0.005$). For functional analysis of the metastasis-specific proteins, we performed an Ingenuity Pathway Analysis and discovered a strong relationship of all candidates with the TGF-β-dependent EMT pathway. Our results demonstrated the potential application of the MALDI-IMS proteomic approach in identifying protein markers of metastasis in PTC. The novel protein markers identified in this study may be used for risk stratification regarding metastatic potential in PTC.

M. Nipp · H. Zitzelsberger (✉)
Department of Radiation Sciences, Research Unit of Radiation
Cytogenetics, Helmholtz Zentrum München-German Research
Center for Environmental Health GmbH,
Ingolstaedter Landstraße 1,
85764 Neuherberg, Germany
e-mail: zitzelsberger@helmholtz-muenchen.de

M. Elsner · B. Balluff · S. Meding · S. Rauser · H. Höfler ·
A. Walch
Institute of Pathology, Helmholtz Zentrum München-German
Research Center for Environmental Health GmbH,
Neuherberg, Germany

B. Balluff
Department of Medicine II, Klinikum rechts der Isar,
Technische Universität München,
Munich, Germany

H. Sarioglu · M. Ueffing
Research Unit of Protein Science,
Helmholtz Zentrum München-German Research Center
for Environmental Health GmbH,
Neuherberg, Germany

K. Unger
Human Cancer Studies Group,
Department of Surgery and Cancer,
Hammersmith Hospital, Imperial College London,
London, UK

H. Höfler
Institute of Pathology, Technische Universität München,
Munich, Germany

Introduction

Among all thyroid cancers, papillary thyroid carcinoma
(PTC) is the most common well-differentiated cancer and
accounts for approximately 80–85% of all thyroid malig-
nancies [1, 2]. Lymphatic metastasis develops in approxi-
mately 30–80% of PTC patients [3, 4]; it can even be found
in very low-risk micro-PTC [5]. Recent studies have
demonstrated that the presence of cervical lymph node
metastasis is a significant prognostic factor for the
recurrence of the disease [3, 5]. This finding has significant
clinical relevance because tumor recurrence at the neck
accounts for one third of all PTC-related deaths. There is
no effective treatment for radioiodine-resistant metastatic
disease [6], which is demonstrated by a 10-year survival
rate of only 10% [2].

Considering the poor outcome in this PTC subgroup,
molecular characterization of the metastatic phenotype of
PTC and elucidation of its association with aggressive
clinical behavior are needed for the development of new
therapeutic strategies and for improving the patient risk
stratification. Considering epigenetic and genetic alterations
as the forces that drive carcinogenesis, genomic studies
have provided valuable information regarding the genetic
features of PTC [7, 8]. Proteomic approaches have opened
a new avenue into the pathogenesis of PTC as the
phenotype of a cell is determined by proteins and cannot
be precisely predicted based on genomic features alone.
Moreover, protein expression levels may be poorly correlated
to messenger RNA expression levels [9]; post-translational
modifications, such as phosphorylation, glycosylation, and
proteolytic processing, can significantly modify the functions
of proteins and the disease-specific characteristics of the cell
or tissue in which the protein is expressed.

Matrix-assisted laser desorption/ionization (MALDI)
imaging mass spectrometry (IMS) is a powerful tool for
the investigation of protein expression patterns via the
direct (in situ) analysis of tissue sections [10]. This method
has advantages over other proteomic approaches that
require tissue homogenization because it is based on the
cell morphology [11]. It allows the direct evaluation of
tumor cells, the determination of correlations with other
morphologic features such as tumor subtype, and the
investigation of small tumor tissue specimens [12]. Based
on these features, MALDI-IMS is a valuable tool for tissue
analysis and molecular histology [13]. In addition, it can be
used to determine the distribution of hundreds of molecules
in a single measurement without the requirement for
specific protein labeling [14]. MALDI-IMS has great

potential for use in oncology research due to its fast and
relatively inexpensive implementation that needs neither
antibodies nor radioactivity because of its non-targeted but
morphology-driven approach making MALDI-IMS suitable
for biomarker discovery experiments. To date, this tech-
nique has been successfully applied to analyze various
types of cancerous tissues, including human non-small cell
lung cancer, glioma, and ovarian, prostate, and breast
cancer [15–17]. Analyses of the resulting complex mass
spectrometry data sets using modern computational tools
have been used to identify the disease state, response
prediction, and patient prognosis-specific protein expres-
sion patterns [18].

In the present study, we analyzed a cohort of patients with
PTC that was matched for size of the primary tumor (pT), age,
gender, and geographical origin to identify metastasis-related
changes in the protein expression patterns of the tumors.
Using this experimental design, we minimized the number of
variables with known genetic effects (e.g., age, gender, and
ethnicity) to reveal metastasis-related changes.

Materials and methods

Sample collection and tissue specimens

Frozen tissues and formalin-fixed paraffin-embedded tissues
from adult papillary thyroid cancer patients (mean age at
surgery, 35.7 ± 7.6 years) were obtained from the Institute of
Radiation Medicine and Endocrinology, Minsk, Belarus. The
study was approved by the Ethics Committee of the Bavarian
General Medical Council (no. 00163) with informed consent
of the patients or their guardians. The specimens were
classified according to the UICC system [19] by pathologists
at the Thyroid Cancer Center, Minsk, and at Martha-Maria
Hospital, Munich. One hundred eighteen patients (29 in the
discovery set and 89 in the validation set) were recruited for
this study. Cases were matched as closely as possible on
tumor size (pT). The vast majority of cases in both tumor
groups (with lymph node metastasis (N1) vs. without lymph
node metastasis (N0)) of the discovery set were pT2 whilst
only four cases were pT4. Thus, the proportion of pT2 cases
compared with pT4 cases is very similar in the discovery and
the validation set of tumors (approx. 80% pT2 cases in each
set). The histomorphological and clinical characteristics of
the analyzed cases are listed in Table 1 as well as more in
detail in Tables 1 and 2 in the Electronic supplementary
material (ESM).

MALDI-IMS analysis

The frozen tissue samples were cryosectioned on conduc-
tive indium-tin-oxide-coated glass slides (Bruker Daltonik

Table 1 Clinical characteristics of the PTC patients

Set characteristics	Discovery set (FT)	Validation set (FFPE)					
	MALDI-IMS	S100A-10 (IHC)		S100-A6 (IHC)		TXN (IHC)	
Mean age (range)	36.7 (30–44)	36.4 (30–46)		36.9 (30–46)		36.6 (30–46)	
No. of patients	29	71[c]		89		79	
No. of female (♀) patients	29	65[c]		79		71	
No. of male (♂) patients	0	6[c]		10		8	
No. of B-RAF-positive patients[a]	3	3		3		3	
No. of B-RAF-negative patients[a]	10	38[c]		46		46	
TNM classification [20]							
pTN0[b]	14 pT2N0	19	4 pT1N0 14 pT2N0 1 pT3N0	26	6 pT1N0 20 pT2N0	20	4 pT1N0 15 pT2N0 1 pT3N0
pTN1[b]	11 pT2N1 4 pT4N1	52	5 pT1N1 40 pT2N1 2 pT3N1 5 pT4N1	63	6 pT1N1 46 pT2N1 2 pT3N1 9 pT4N1	59	5 pT1N1 45 pT2N1 2 pT3N1 7 pT4N1

FT frozen tissue, FFPE formalin-fixed, paraffin-embedded (tissue)

[a] No tumor tissue available for 30 cases of the B-RAF sequencing

[b] MALDI-IMS—more than 86% of pT2 and only females in the set; IHC—more than 74% of pT2 and 90% females in the set; all cases without an observed distant metastasis

[c] Due to technical reasons, eight of 79 patient tissues could not be considered for the final analysis

GmbH, Bremen, Germany), washed briefly in 70% and 100% ethanol, dried, and covered directly with the MALDI matrix (10 mg/ml sinapinic acid (Sigma-Aldrich, Taufkirchen, Germany) in water/acetonitrile 40:60 (v/v) with 0.2% trifluoroacetic acid (Applied Biosystems, Darmstadt, Germany)). The MALDI matrix was applied using an ImagePrep station (Bruker Daltonik GmbH, Bremen, Germany) according to the manufacturer's protocol. The MALDI measurement was performed using an Ultraflex III MALDI-TOF/TOF instrument in linear mode over a mass range of 2,400–25,000 Da and a sampling rate of 0.1 GS/s using the FlexControl 3.0 and FlexImaging 2.1 software packages (Bruker Daltonik GmbH, Bremen, Germany). The lateral resolution of MALDI-IMS was set at 200 μm; 200 laser shots were accumulated per pixel at a constant laser power density. A ready-made protein standard applied directly to the sample carrier was used to calibrate the spectra (Bruker Daltonik GmbH, Bremen, Germany).

Following the MALDI-IMS analysis, the cryosections were incubated in 70% ethanol to remove the matrix and then washed in distilled water. Subsequently, the slides were stained with hematoxylin and eosin (H&E), scanned with the MIRAX DESK system (Carl Zeiss MicroImaging GmbH, Göttingen, Germany), and co-registered with the MALDI-IMS results to correlate the mass spectrometric data with the histological features of the same section.

Protein extraction

Five 5-μm cryomicrotome sections from one frozen tissue sample of case 6 from the pN1 cohort were selected based on the significant MALDI-IMS discriminating peaks of that case. The samples were immersed at a concentration of 200 mg/ml in a protein extraction solution containing 50-mM sodium phosphate buffer (pH 7.4) and Roche Complete Mini Protease Inhibitor Cocktail Tablets (Roche Applied Science, Indianapolis, IN). The tissue samples were manually homogenized on ice followed by sonication on ice (ten times for 30 s each). The homogenates were centrifuged at 12,000 rpm in a benchtop centrifuge at 4°C for 30 min, and the supernatant was further processed. The protein extract was precipitated for purification, enriched in 80% acetone overnight at −20°C and analyzed using 1D gel electrophoresis (12% SDS gel). The protein concentration was 100 μg/ml, as measured using the Bradford method with BSA as the protein standard (Sigma-Aldrich, Taufkirchen). All of the samples were stored at −80°C until analysis.

One-dimensional gel electrophoresis

A 12% SDS gel was prepared using a standard protocol [20] and 100 μg of the sample were applied to the gel. For staining, we used 0.4% Coomassie Brilliant Blue R250 (Serva Electrophoresis GmbH, Heidelberg, Germany) in 50% methanol and 12% acetic acid. In-gel digestion with trypsin was performed according to published procedures [21].

MS analysis and protein database search

After the SDS-PAGE bands were cut out and digested with trypsin, the resulting peptides were separated on a

nano-RP-HPLC column (PepMap, LC Packings, Sunnyvale, CA, USA) connected to a linear quadrupole ion trap mass spectrometer (LTQ Orbitrap XL, Thermo Scientific, Waltham, MA, USA) equipped with a nano-ESI ion source. All of the obtained MS/MS spectra were used as input for searches in the UniRef100 human sequence database using Mascot (v2.2.06, Matrix Science, London, UK). A final evaluation of the protein/peptide identification results was performed within the Scaffold 3 software framework (Proteome Software, Portland, OR, USA).

Immunohistochemistry

For immunohistochemical validation of the selected proteins, the sections of a tissue microarray containing 89 formalin-fixed, paraffin-embedded tissues cores in triplicates were prepared and incubated with the following primary antibodies: mouse anti-S100-A10 (p11, the calpactin light chain) mono-clonal antibody (Swant, Bellinzona, Switzerland; 1:50,000, 0.2 μg/mL), rabbit anti-S100-A6 Ab-9 polyclonal antibody (Thermo Scientific, Waltham, MA, USA; 1:200, 0.5 μg/mL) and thioredoxin-1 rabbit monoclonal antibody (Cell Signaling, Beverly, MA; 1:500, 0.1 μg/ml). Detection was performed using peroxidase-DAB (diaminobenzidine)-MAP chemistry with an automated stainer (Ventana Discovery XT, Ventana, Tuscon, AZ, USA).

The intensity of the staining was scored as follows: completely negative (0), slightly stained (1), moderately stained (2), and strongly stained (3). Scores of 0 and 1 were considered negative (−), whereas scores of 2 and 3 (+) were considered positive. The differences between the immunohistochemical scores were analyzed using Fisher's exact test. P values of <0.05 were considered significant. All of the statistical tests were performed using the R software package.

B-RAF (V600E) sequencing

To determine the presence of the T1796 mutation of the *B-RAF* gene (T1796A), 100 ng of genomic DNA was amplified using primers that spanned exon 15, as described by Powell et al. [22]. After verifying the size of the amplification product, the DNA was purified using a QIAquick PCR Purification Kit (Qiagen, Hilden, Germany) and analyzed for the mutation using a BigDye kit (Applied Biosystems) in combination with an ABI3730xl capillary electrophoresis DNA analyzer (Applied Biosystems). The fluorograms were assessed using UGENE software (Unipro, Novosibirsk, Russia).

Statistical analyses

Tumor-associated spectra were selected using FlexImaging 2.1 software (Bruker Daltonik GmbH, Bremen, Germany).

For this purpose, we defined in every tissue section regions of interest (ROIs) that contained papillary thyroid cancer tissue cell populations. One hundred of these extracted mass spectra were randomly selected for each case and processed further. This processing included recalibration, normalization based on the total ion count, and peak identification, using ClinProTools 2.2 software (Bruker Daltonik GmbH, Bremen, Germany). Significant differences in peak intensity between the groups without and with metastasis (pT2N0 and pT2N1/pT4N1) were determined using the Wilcoxon rank-sum test with a significance cutoff of 0.05.

Unsupervised hierarchical clustering of all samples was performed within the R statistical environment (R Development Core Team, 2009) using McQuitty linkage and the Canberra distance measurement between protein profiles.

Protein set enrichment analysis

Protein set enrichment analysis was performed using Ingenuity Pathway Analysis (Ingenuity Systems, Mountain View, CA). The list of proteins (92) that were found to be overexpressed in the node-positive PTC compared with node-negative PTC by MALDI-IMS was uploaded to the Ingenuity Pathway Analysis website (www.ingenuity.com) and analyzed using default parameters. P values smaller than 0.05 with a false discovery rate smaller than 0.25 were accepted as statistically significant.

Results

Determination of discriminating expression profiles between pT2N0 and pT2/4N1 PTC

To detect proteomic patterns that were associated with lymph node status in thyroid tumors, we assessed the protein profiles of a discovery set ($n=29$) and a validation set ($n=89$) using MALDI-IMS and IHC, respectively. The same tissue sections analyzed by MALDI-IMS were stained with H&E, and the digital images were co-registered with the MALDI-IMS results to correlate the mass spectrometric data with the histological features. This procedure allowed a histology-directed analysis of the mass spectra obtained from the measured tissue samples.

To identify these proteomic mass patterns, we performed an LC-MS/MS analysis. Proteins were extracted from tissue and the complexity of the sample was reduced by 1D gel electrophoresis. A slice of the low molecular weight fraction was cut out, digested with trypsin, and analyzed with LC-MS/MS. The resulting significant protein hits and their intact protein masses were then compared with the differentially expressed protein mass features of MALDI-

IMS results. Validation of candidate proteins was performed with IHC on a validation set.

The co-registration of discriminating peaks and H&E stained tissue is illustrated in Fig. 1; the typical single mass discriminating peaks for selected spectra differences between tumor areas with and without metastasis are also shown. Based on these promising preliminary results, we defined in every tissue section ROIs that contained papillary thyroid cancer tissue cell populations using the ClinProTools 2.2 software (Bruker Daltonik GmbH, Bremen, Germany).

On average, we resolved 100 to 150 peaks per case within the mass range of m/z 3,000 to 16,000. In total, 36 m/z species were found to discriminate papillary thyroid cancer without lymph node metastasis ($n=14$) from thyroid cancer with lymph node metastasis ($n=15$).

In the initial discovery experiment, we analyzed 29 tumor tissue samples ($n_{pT2N0}=14$, $n_{pT2N1}=15$), among which 36 individual m/z species, representing specific pN1 or pN0 tumor cell populations defined by the chosen ROIs, were used for the comparative analysis. These 36 m/z species are m/z 3,327, 5,651, 5,994, 6,295, 6,315, 6,449, 6,856, 6,886, 6,919, 6,954, 8,453, 8,489, 8,537, 8,625, 8,657, 9,264, 10,094, 10,130, 10,173, 10,211, 10,254, 10,294, 10,324, 10,360, 10,398, 10,496, 11,184, 11,310, 11,347, 11,383, 11,567, 11,608, 11,649, 13,789, 13,828, and 13,897 and discriminated between the pN1 and the pN0 tumor samples.

The McQuitty Agglomeration Algorithm and Canberra distance identified two clusters: one cluster contained only the pT2/4N1 samples, whereas the other cluster contained only the pT2N0 cases, excluding a single false-positive case in each group. Representative m/z species and visualized unsupervised clustering using spectral grouping are shown in Table 2 as well as in Fig. 2.
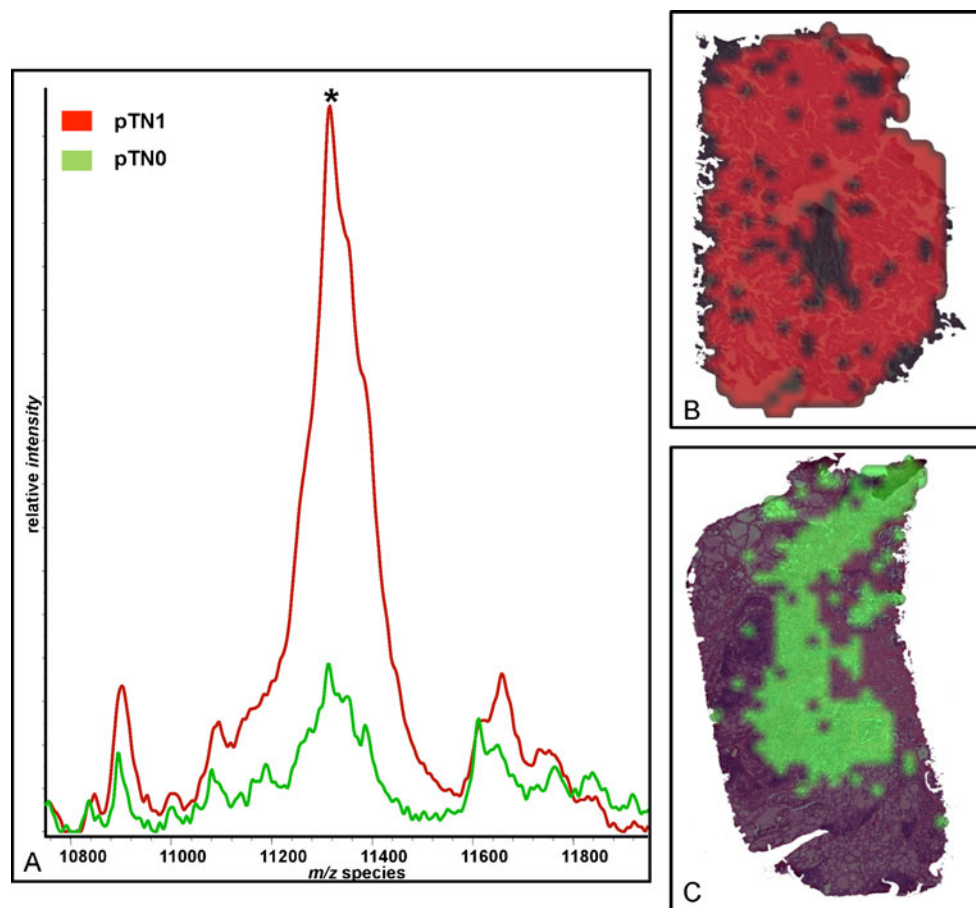

Fig. 1 MALDI-IMS analysis of PTC. **a** Direct tissue mass spectrometric analysis reveals tissue-type-specific profiles, as shown in this comparison of papillary thyroid cancer tissues (PTC) without (pN0) and with lymph node metastasis (pN1) from $n=29$ individual patient samples that were analyzed by MALDI-IMS. The overall average spectra shown in the mass range of 10,770–11,970 Da (x-axis) were obtained from PTC pN0 (green) and PTC pN1 (red) tissue areas. An example of differentially expressed m/z species (m/z 11,310) is indicated by an *asterisk*. Similar figures showing the m/z species of our three candidates in detail can be found in the ESM. **b** Overlay of H&E-stained tissue and tumor-specific m/z species after unsupervised clustering. Only the *red* area was considered tumor tissue area of a pT2N1 case and was used for the analysis. **c** Overlay of H&E-stained tissue and tumor-specific m/z species after unsupervised clustering. Only the *green* area was considered tumor tissue of a pT2N0 case and was used for the analysis

Table 2 Thirty-three discriminating *m/z* species overexpressed in pT2/4N1 detected by MALDI-IMS

m/z species MALDI-IMS	Theoretical mass weight	Δ*m*	Protein name
5,651	5,655	4	Beta-defensin 110
5,994			
6,295	6,297	2	Beta-defensin 130
6,315			
6,449			
6,856			
6,886	6,886	0	FAM165B
6,919			
6,954			
8,453			
8,537	8,542	5	Interleukin-8
8,625			
8,657	8,658	1	CAMK2N2
10,094[c]	10,094[c]	0[c]	S100-A6[b]
10,130			
10,173			
10,211			
10,254			
10,294			
10,324			
10,360			
10,398	10,400	2	S100-P
10,496			
11,184	11,187	3	S100-A10[a, b]
11,310			
11,347			
11,383			
11,567			
11,608	11,606	2	TXN[a, b]
11,649			
13,789	13,789	0	HIST2H2BE
13,828	13,833	5	PHPT1
13,897			

[a] Proteins were identified by LC-MS/MS and could be correlated to corresponding masses derived from MALDI-IMS approaches. In order to confirm these protein hits, they were further validated by IHC

[b] Proteins were further validated by IHC

[c] The mass weight described by Sanders et al. 2008 [24] was 10,094 and should most probably represent the S100A6 molecule without starting methionin and with calcium bound

[d] A 5 Da was considered as MALDI-IMS measurement accuracy

Protein identification

Protein identification after the discovery of significance in the clinical context remains a challenge for MALDI-IMS. Although peptide identification by MALDI-IMS is more difficult than by LC-MS/MS, the direct identification of

tumor-specific peptides with a high molecular weight (e.g., 4,300 Da) has been demonstrated [23]. Because the masses of the detected discriminating proteins were in the range of 4,000–14,000 Da, we chose a different identification strategy.

To identify these proteomic mass patterns, we performed an LC-MS/MS analysis on case 6. Proteins were extracted from tissue and the complexity of the sample was reduced by 1D gel electrophoresis. A slice of the low molecular weight fraction was cut out (see Fig. 3 in the ESM), digested with trypsin and analyzed with LC-MS/MS. The resulting significant protein hits and their intact protein masses were then compared with the differentially expressed protein mass features of MALDI-IMS results. Ninety-two proteins were identified in the selected 1D gel band with a probability of at least 95%. Two of these proteins (S100-A10 and thioredoxin) were identified as mass discriminating *m/z* species for pT2N1 tumor tissues before. Validation of candidate proteins was performed with IHC on a validation set. Because of the identification of four strong related S100-proteins and the formerly published identification of *m/z* 10,094 as S100-A6 by Sanders et al. [24] S100-A6 was analyzed by IHC on the same validation set.

Overexpression of S100-A6, S100-A10, and TXN confirmed by immunohistochemistry

The three candidate proteins S100-A10 (p11, the ligand of Annexin-II), S100-A6 (Calcyclin) and TXN (thioredoxin) were further validated using IHC. In case of S100-A6 and S100-A10, this validation was in particular important because of a similar range of *m/z* species and conserved protein domains within the S100 protein family. Therefore, the monoclonal antibody mouse anti-S100-A10 (Swant, Bellinzona) and the rabbit anti-S100-A6 Ab-9 polyclonal antibody (Thermo Scientific, Waltham, MA, USA) were chosen that are specific for one single S100 protein without any known cross-reactions with other S100 family members. Whereas antibody staining was nearly absent in all of the normal thyroid tissues, positive staining was detected in more than 50 of the 89 tumor cases (Table 3; Fig. 3). A correlation analysis of the immunohistochemical staining results with clinical data revealed that the overexpression of S100-A10, S100-A6, and TXN was associated with metastasis (*p* value for S100A10: 0.00018; *p* value for S100-A6: 0.0013; *p* value for TXN: 0.00003; Fisher's exact test). There was a high overlap because more than 85% of the stained pN1 cases were positive for all three tested antibodies. The positive predictive value was between 85% (S100-A6) and 89% (S100A10), the negative predictive value between 54% (S100-A10) and 71% (TXN). Because of a high overlap in overexpression of
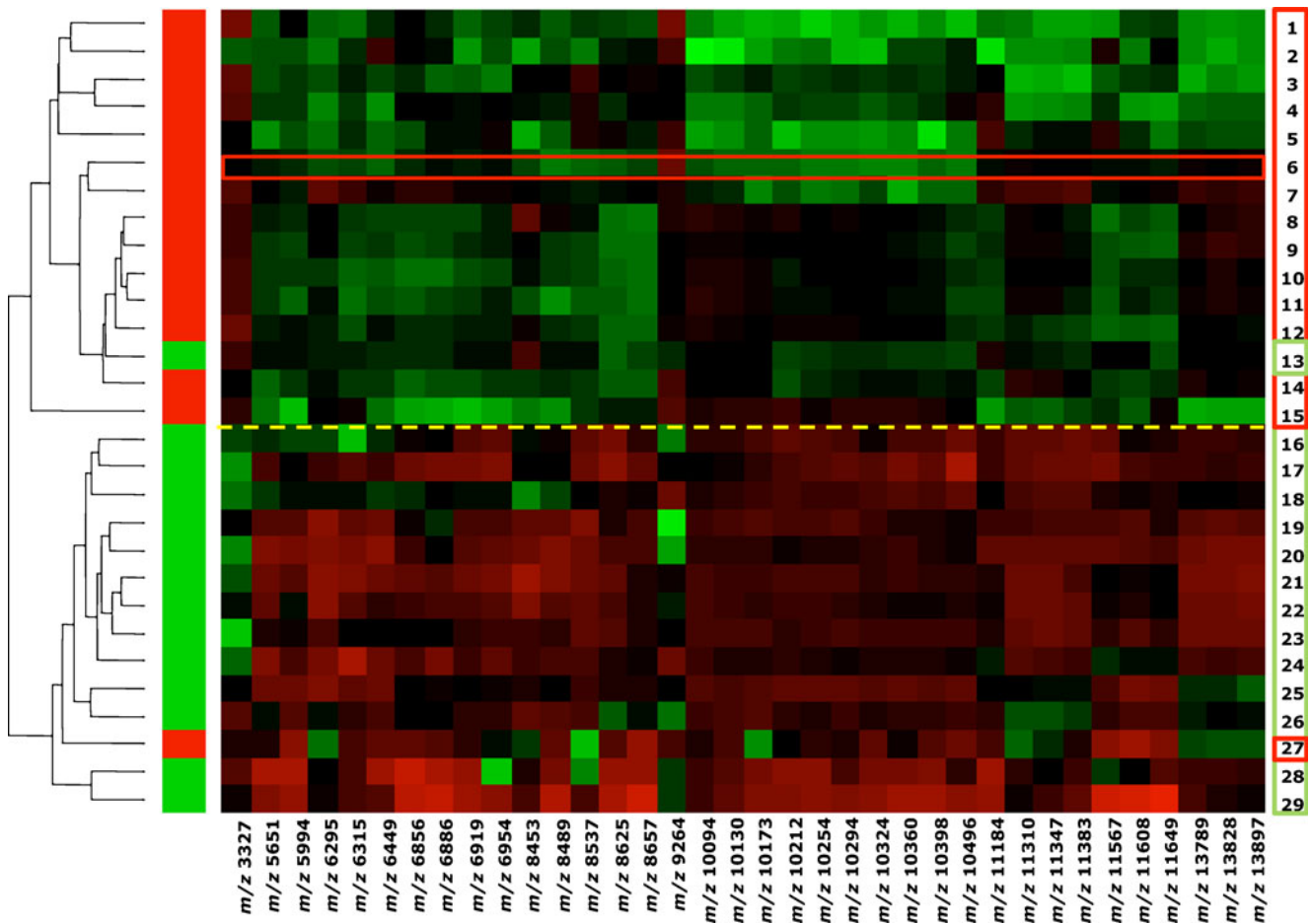
Fig. 2 Heatmap of all 29 tumor tissues that were analyzed by MALDI-IMS after unsupervised hierarchical clustering. The number of the patient is shown on the *right*; the corresponding color code is shown on the *left* (*red*, pT2N1; *green*, pT2N0). The 36 discriminating mass species are shown at the *bottom* (*from left to right*; corresponding *m/z* species to our validated candidate proteins are *red highlighted and underlined*). The *green rectangles* indicate overexpression of a specific *m/z* species in one tissue; *red* indicates diminished expression. *Less intensive rectangles* indicate a greater difference in expression compared with the *darker* ones. Our three candidates (*m/z* 10,094, 11,184, and 11,608) were altogether overexpressed in four cases, two of them together in seven (*m/z* 10,094 and 11,184) and 11 cases (*m/z* 11,184 and 11,608) of the pT2N1 group. Case 6 was chosen for further LC-MS/MS because of its most typical pT2N1-spectra profile with strong overexpression of metastasis-specific *m/z* species. Most of the *m/z* species were over-represented in metastatic patients, which resulted in the proteomic pattern that separated pT2N0 from pT2N1 (*p* value, 0.00003)

these proteins and similar classification values, one single antibody shows nearly the same PPV as combination of these proteins while the S100-A10 antibody shows best PPV and TXN antibody shows best NPV.

S100-A-10 antibody is also suggested because of its very well technical staining results. The small percentage of available pN0 cases might contribute significantly to the lower NPV in all three experiments.

Table 3 Results obtained for the discovery and validation sets

Antibody	Discovery set (MALDI-IMS)		Validation set (IHC)					
	n.a.		S100-A10		S100-A6		TXN	
Cluster/score	N0	N1	0/−	1/±	0/−	1/±	0/−	1/±
pT2N0	13	1	14	5	17	9	15	7
pT2N1	1	14	12	40	13	50	6	51
p value	0.00003[a]		0.00018[a]		0.0013[a]		0.00003[a]	
PPV[b]	93.33%		88.88%		84.75%		87.93%	
NPV[c]	92.87%		53.85%		56.67%		71.42%	

[a] Fisher's exact test
[b] Positive predictive value
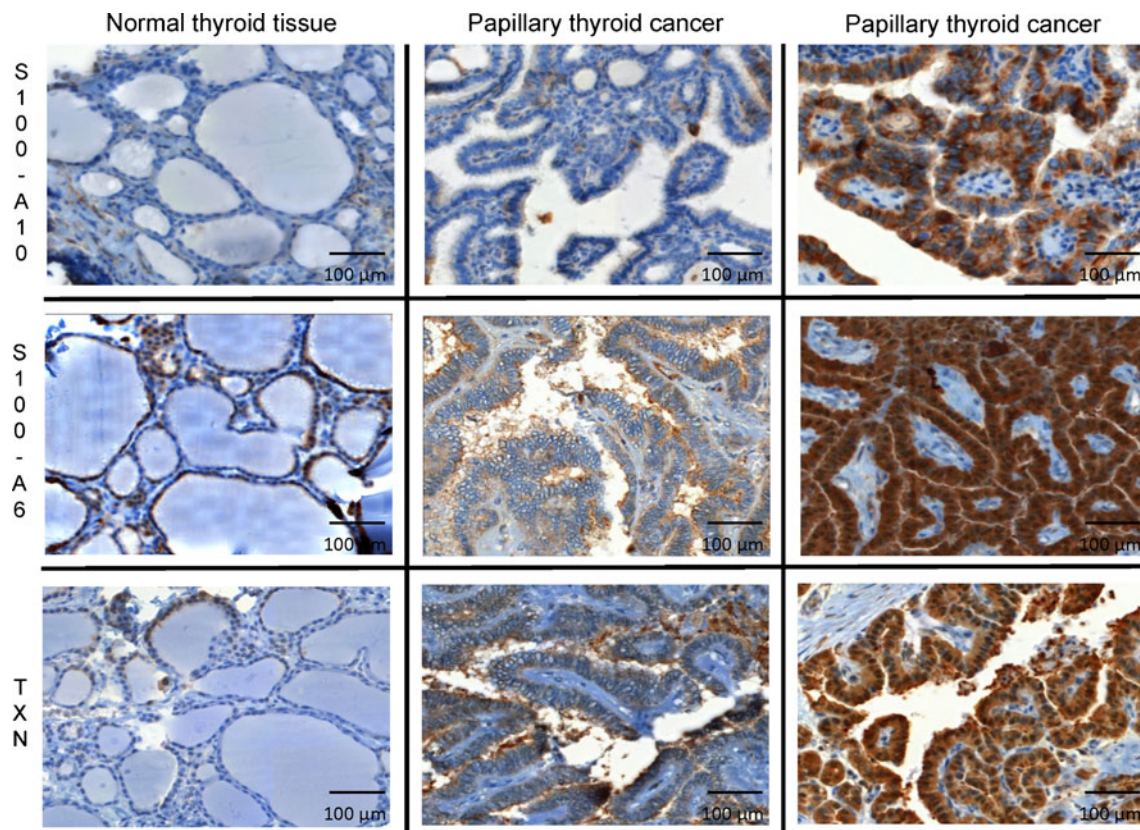[c] Negative predictive value

Fig. 3 Representative immunohistochemical staining of S100-A10, S100-A6, and TXN in normal thyroid (*left side*) and tumor tissues (*from top to bottom*: S100-A10, S100-A6, thioredoxin; *from left to right*: normal thyroid tissue (score, −), papillary thyroid tissue (score, −), and papillary thyroid tissue (score, +)

B-RAF mutation V600E

Sixty of 118 tumors were characterized for the presence of the *B-RAF* (V600E) mutation. Among the characterized tumors, 54 cases (90%) did not carry the *B-RAF* (V600E) mutation, whereas six cases (10%) were positive for this mutation. We could not find any statistical relationship between overexpression of one of our three candidates and *B-RAF* (V600E) mutation that may be up to statistical problems concerning the small number of *B-RAF* (V600E) positive patients in this cohort.

Pathway enrichment analysis

In order to identify pathways that are specifically deregulated in metastatic PTC the candidate proteins identified using MALDI-IMS (Table 2) were subjected to a protein set core analysis. Significantly over-represented pathways associated with the candidate proteins were the TGF-β-depending epithelial–mesenchymal transition (EMT) (Fig. 4) and the actin cytoskeleton signaling pathway. Interestingly, 11 out 92 (12%) of the proteins that were specifically upregulated in node-positive compared with node-negative tumors identified by LC-MS/MS in one of the node-positive

cases (case 6) are part of the TGF-β-dependent EMT and actin cytoskeleton pathways.

Discussion

The majority of PTC cases demonstrate a slow growth and an excellent overall prognosis [4]. Despite this favorable clinical outcome, approximately 15% of PTC cases demonstrate a more aggressive behavior and present local invasion, treatment resistance, recurrence and distant metastases [25]. Lymph nodes are the most frequent metastatic sites in PTC; lymph node metastasis indicates a high risk for disease recurrence and poor survival [26]. Therefore, it is important to identify biomarkers that indicate an aggressive outcome in PTC. The ability to detect such biomarkers in blood or serum would potentially improve the treatment in finding high-risk groups for recurrence.

To identify biomarkers in tumor tissues, we investigated the proteomic profiles of PTC cases with or without lymph node metastasis that were matched for the following: age at diagnosis, gender, ethnicity, and tumor size. This carefully matched cohort allowed us to employ an advanced

Fig. 4 TGF-β-related pathway generated from our candidate proteins using Ingenuity Pathway Analysis (*lime green*—proteins detected by MALDI-IMS, identified by LC-MS/MS, and validated using IHC (Table 2); *dim gray*—proteins identified by LC-MS/MS on case 6 (Table 3 in the ESM); *yellow arrows* indicate direct relationship between TGF-β and one of our identified proteins
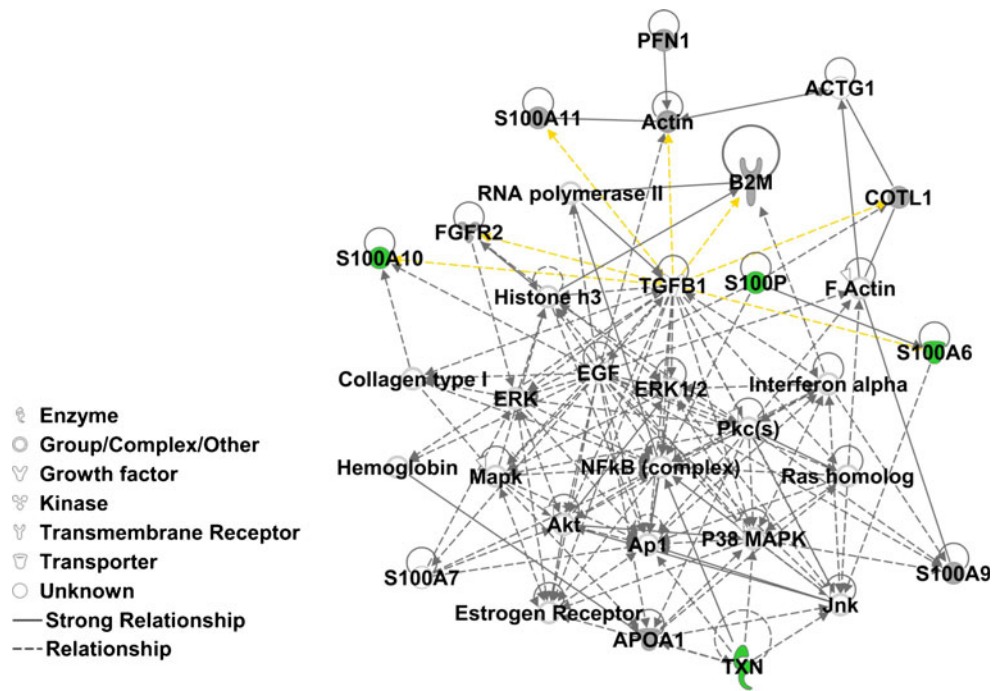
MALDI-IMS approach to identify 36 *m/z* species that discriminated metastatic from non-metastatic tumor cases in a discovery cohort (Fig. 2). Interestingly, three proteins, S100-A6, TXN, and S100-A10, were found to represent molecular markers of metastasis in PTC. This finding was confirmed by the overexpression of these proteins in lymph node-positive PTC in an independent validation cohort.

Thus far, the most prominent prognostic marker in PTC for disease recurrence, progression, and metastasis is the *B-RAF* mutation (V600E). Several studies have reported a correlation of this marker with tumor invasion and metastasis [27], with radioactive iodine-refractory and FDG-PET-positive differentiated thyroid cancers [28], and its use for preoperative risk stratification in papillary thyroid cancer [7]. Although the *B-RAF* (V600E) mutation has been established as a prognostic risk factor, the correlation between its occurrence and advanced PTC is not obvious because only 36% of *B-RAF* (V600E)-positive tumors have demonstrated disease recurrence, whereas 12% of *B-RAF* (V600E)-negative tumors also present advanced PTC [7]. Thus, the mechanism by which *B-RAF* (V600E) induces tumor aggressiveness remains unclear. It was shown recently that *B-RAF* (V600E) mutation is associated with epithelial–mesenchymal transition papillary thyroid cancer [29]. In the present study, only a small portion of the N1 cases harbored the *B-RAF* (V600E) mutation; therefore, *B-RAF* (V600E) is unlikely to play an important role in tumor aggressiveness according to our tumor cohort. This finding strongly supports the search efforts for biomarkers among other gene alterations, such as TSP-1, that are also important for tumor invasion and metastasis [27].

To date, several other biomarkers have been tested for their potential to predict lymph node involvement in PTC [30–32]; however, none of them have entered clinical practice, which could be due in part to the use of inappropriately matched tumor cohorts in previous studies. To reduce the variability of the experimental data to a maximum, we matched the tumors of the discovery set according to as many parameters as possible (such as age, gender, and tumor size). Using this study design revealed S100-A6, TXN, and S100-A10 as novel candidate biomarkers for metastasis in PTC. Moreover, to our best knowledge, this report is the first to identify proteomic markers of lymph node metastasis in PTC. We also demonstrated the potential of using MALDI-IMS to detect differences in proteomic patterns among tumor groups based on an in situ analysis of the tissue sections and showed its significantly higher accuracy and sensitivity in predicting tumor subgroups than normally found in classic approaches like IHC which is a result of its semi-quantitative abilities. Our strategy to compare PTC cases that were highly matched and that only differed with respect to lymph node involvement differs from the strategies used in other studies that compared either different variants of PTC (aggressive tall-cell variants vs. indolent conventional PTC [32] or primary PTC and the corresponding lymph node metastasis [33] at the mRNA level. Interestingly, in the study reported by Wreesmann et al., MUC1 was identified as a potential biomarker for the aggressive behavior of PTC; they also demonstrated the genomic amplification and dysregulation of MUC1 at the mRNA level and the overexpression of MUC1 protein by

immunohistochemistry [32]. MUC1 is located in chromosome band 1q21, which is very close to the loci of two candidate biomarkers identified in the present study: S100-A10 and S100-A6, mapped to chromosome bands 1q21.3 and 1q23, respectively. Considering this genetic association, the chromosomal region 1q21–1q23 is likely important for tumor aggressiveness in PTC.

The present study identified three novel protein markers for metastasis in PTC: S100-A10, TXN, and S100-A6. In initial IHC experiments on five pT2N1 patients of our discovery set, we could observe a correlation in overexpression of these candidate proteins between the lymph node metastases and their primary tumors (Fig. 2 in the ESM). Overexpression of S100-A6 has been reported in several types of cancer such as hepatocellular carcinoma [34], malignant melanoma [35], and in papillary thyroid carcinoma. In contrast, a reduced expression was observed in anaplastic thyroid carcinomas and in normal thyroid tissue [36, 37]. Further, a correlation of S100-A6 expression level and the tumor grade was observed in colorectal cancer [38] and pancreatic cancer [39] [40]. In primary colorectal cancer lesions, an overexpression was detected at the invading fronts and in liver metastases. These observations suggest that S100-A6 could be involved in the stimulation of tumor cell invasion [38]. Since S100-A6 expression was detected both in tumor and stroma cells, it has been proposed that S100-A6 regulates pulmonary fibroblast proliferation [41]. Therefore it is likely that S100-A6 also might modulate tumor progression by regulating proliferation of tumor-associated fibroblasts. In papillary thyroid carcinoma, Sofiadis et al. reported different isoforms of S100-A6 using LC-MS/MS analysis and showed that PTC can be distinguished from follicular thyroid tumors only by the S100-A6 biomarker [42]. In this study, the expression of S100-A6 was in reported to be independent from the presence of *B-RAF*-mutations.

S100-A10, the second candidate protein, binds to tissue plasminogen activator (tPA) and plasminogen, thereby stimulating the tPA-dependent plasmin production. S100-A10 also co-localizes plasminogen with the urokinase-type plasminogen activator (uPA)-uPAR complex, which results in the stimulation of uPA-dependent plasmin formation on the surface of cancer cells. A loss of S100-A10 from the extracellular surface of cancer cells results in a significant loss of plasmin formation. Moreover, S100-A10 knockdown in tumor cells leads to a dramatic decrease in extracellular matrix degradation and invasiveness as well as reduced metastasis [43]. It is widely accepted that the plasminogen activation system plays a central role in mediating cancer progression [44]. The plasminogen activation system has been extensively studied as a target for anticancer therapy using a variety of approaches [45]. The key role of S100-A10 in regulating plasminogen

activation makes it an attractive target for the development of novel cancer therapies.

The protein TXN is an oxidoreductase enzyme that contains a dithiol-disulfide active site. Experimental studies have suggested that TXN is an important regulator of the G1 phase of the cell cycle that functions by regulating cyclin D1 transcription and the ERK1/2/AP-1 signaling pathways [46]. Furthermore, TXN contributes to many functional hallmarks of cancer, including increased proliferation, resistance to cell death and increased angiogenesis. TXN expression is associated with aggressive tumor growth, therapy resistance and decreased patient survival [47]. Moreover, the A2-S100-A10 complex is a substrate for TXN [43] and therefore, it is also directly associated with plasmin production.

Notably all three proteins are part of the TGF-β-dependent EMT pathway (Fig. 4). Thus, these proteins are linked to network that controls the EMT in tumors. In this network, TGF-β plays a complex but not entirely known role: it may function both as a tumor suppressor in early stages of tumor development and as tumor promoter in late stages of tumor progression [48, 49]. TGF-β promotes tumor progression and metastasis by exerting pleiotropic effects on the neoplastic cells, including induction of EMT, and on the surrounding stroma [50]. Increased expression of TGF-β occurs in many human cancers and correlates with enhanced invasion and metastasis. [51, 52] One of the key events during the transition of an epithelial cell into a mesenchymal cell is the so-called robust remodeling of the actin cytoskeleton. As demonstrated in Fig. 4, functional pathway analysis identified cytoskeletal reorganization as one of the major processes regulated by the proteins that we identified in our study. The candidate proteins, S100-A10 and S100-A6, were shown to be overexpressed in metastasized PTC by MALDI-IMS while ACTG1 and COTL1 were identified to be present in one pT2N1 case using LC-MS/MS. S100-A6 and S100-A10 which were furthermore validated by immunohistochemistry are known to be involved in the temporal regulation of actin cytoskeleton remodeling at the leading edge of a migratory cells. Both S100-A6 and S100-A10 are directly regulated by TGF-β. Feighery et al. [53] reported that S100-A6 could play an important role in immune mediated renal EMT and the ensuing fibrosis as well as in other TGF-β-dependent cellular EMT-processes like other S100-proteins. Several reports indicate cooperation of TGF-β and Ras/MAPK pathways in promoting EMT. Moreover a study by Grande et al. [54] has shown that EGF-dependent activation of Ras/MAPK stimulates TGF-β-induced EMT.

A major defining characteristic of the plastic response of human epithelial tumor cells to EMT-inducing growth factors is the expression of stromal remodeling proteases and their specific inhibitors. Activation of the serine

protease plasminogen (a prominent component of the epidermal matrix) to the broad-spectrum protease plasmin provides a fundamental mechanism for initiating extracellular matrix proteolysis [55]. This system is regulated by the accessibility of activators and inhibitors at the cell surface, as well as in the pericellular environment. High expression of the uPA and its receptor uPAR have been linked to poor prognosis in cancer patients [56].

In conclusion, using MALDI-IMS, we identified the novel proteomic biomarkers S100-A6, TXN, and S100-A10 in addition to 33 yet unreported candidate proteins in metastatic PTC. These markers may be important for risk stratification and are potential targets for the development of novel therapeutic strategies. Additional studies are required to understand the complex role of these candidates and the influence of TGF-β-induced EMT on tumor aggressiveness and migration. Therefore, a suitable knockdown model on these three candidates would be very interesting. Another approach could be to look over patient's serum for the presence of our candidate proteins.

References

1. Davies L, Welch HG (2006) Increasing incidence of thyroid cancer in the United States, 1973–2002. JAMA 295:2164–2167
2. Baudin E, Schlumberger M (2007) New therapeutic approaches for metastatic thyroid carcinoma. Lancet Oncol 8:148–156
3. Mazzaferri EL, Jhiang SM (1994) Long-term impact of initial surgical and medical therapy on papillary and follicular thyroid cancer. Am J Med 97:418–428
4. Shaha AR (2000) Controversies in the management of thyroid nodule. Laryngoscope 110:183–183
5. Chow S-M, Law SCK, Chan JKC, Au S-K, Yau S, Lau W-H (2003) Papillary microcarcinoma of the thyroid—prognostic significance of lymph node metastasis and multifocality. Cancer 98:31–40
6. Mehta RS, Negin B, Popii V, Langer C (2008) An aggressive radio-resistant papillary thyroid cancer. Clin Adv Hematol Oncol 6:761–767
7. Xing M, Clark D, Guan H, Ji M, Dackiw A, Carson KA, Kim M, Tufaro A, Ladenson P, Zeiger M et al (2009) BRAF Mutation Testing of Thyroid Fine-Needle Aspiration Biopsy Specimens for Preoperative Risk Stratification in Papillary Thyroid Cancer. J Clin Oncol 27:2977–2982
8. Kimura ET, Nikiforova MN, Zhu Z, Knauf JA, Nikiforov YE, Fagin JA (2003) High prevalence of BRAF mutations in thyroid cancer. Cancer Res 63:1454–1457
9. Chen G, Gharib TG, Huang C-C, Thomas DG, Shedden KA, Taylor JMG, Kardia SLR, Misek DE, Giordano TJ, Iannettoni MD et al (2002) Proteomic Analysis of Lung Adenocarcinoma. Clinical Cancer Research 8:2298–2305
10. Reyzer ML, Caldwell RL, Dugger TC, Forbes JT, Ritter CA, Guix M, Arteaga CL, Caprioli RM (2004) Early changes in protein expression detected by mass spectrometry predict tumor response to molecular therapeutics. Cancer Res 64:9093–9100
11. Cazares LH, Troyer D, Mendrinos S, Lance RA, Nyalwidhe JO, Beydoun HA, Clements MA, Drake RR, Semmes OJ (2009) Imaging mass spectrometry of a specific fragment of mitogen—activated protein kinase/extracellular signal-regulated protein kinase kinase 2 discriminates cancer from uninvolved prostate tissue. Clin Cancer Res 15:5541–5551
12. Deininger S-O, Ebert MP, Fütterer A, Gerhard M, Rocken C (2008) MALDI imaging combined with hierarchical clustering as a new tool for the interpretation of complex human cancers. J Proteome Res 7:5230–5236
13. Hanselmann M, Kirchner M, Renard BY, Amstalden ER, Glunde K, Heeren RMA, Hamprecht FA (2008) Concise representation of mass spectrometry images by probabilistic latent semantic analysis. Anal Chem 80:9649–9658
14. Hanselmann M, Köthe U, Kirchner M, Renard BY, Amstalden ER, Glunde K, Heeren RMA, Hamprecht FA (2009) Toward digital staining using imaging mass spectrometry and random forests. J Proteome Res 8:3558–3567
15. Schwamborn K, Krieg RC, Reska M, Jakse G, Knueche lR, Wellmann A (2007) Identifying prostate carcinoma by MALDI-imaging. Int J Mol Med 20(2):155–159
16. Wolff AC, Hammond MEH, Schwartz JN, Hagerty KL, Allred DC, Cote RJ, Dowsett M, Fitzgibbons PL, Hanna WM, Langer A et al (2007) American Society of Clinical Oncology/College of American Pathologists Guideline Recommendations for Human Epidermal Growth Factor Receptor 2 Testing in Breast Cancer. J Clin Oncol 25:118–145
17. Villanueva J, Shaffer DR, Philip J, Chaparro CA, Erdjument-Bromage H, Olshen AB, Fleisher M, Lilja H, Brogi E, Boyd J et al (2006) Differential exoprotease activities confer tumor-specific serum peptidome patterns. The Journal of clinical investigation 116:271–284
18. Bauer JA, Chakravarthy AB, Rosenbluth JM, Mi D, Seeley EH, Matos Granja-Ingram N, Olivares MG, Kelley MC, Mayer IA, Meszoely IM et al (2010) Identification of Markers of Taxane Sensitivity Using Proteomic and Genomic Analyses of Breast Tumors from Patients Receiving Neoadjuvant Paclitaxel and Radiation. Clinical Cancer Research 16:681–690
19. UICC (2002) In: Sobin LH, Wittekind C (eds) TNM classification of malignant tumours (German edition). Wiley, New York, pp. 59–62
20. Laemmli UK (1970) Cleavage of structural proteins during the assembly of the head of bacteriophage. Nature 227:680–685
21. Hellman U, Wernstedt C, Gonez J, Heldin C-H (1995) Improvement of an "in-gel" digestion procedure for the micropreparation of internal protein fragments for amino acid sequencing. Anal Biochem 224:451–455
22. Powell N, Jeremiah S, Morishita M, Dudley E, Bethel J, Bogdanova T, Tronko M, Thomas G (2005) Frequency of BRAF T1796A mutation in papillary thyroid carcinoma relates to age of patient at diagnosis and not to radiation exposure. J Pathol 205:558–564
23. Rauser S, Marquardt C, Balluff B, Deininger Sr-O, Albers C, Belau E, Hartmer R, Suckau D, Specht K, Ebert MP et al (2010) Classification of HER2 Receptor Status in Breast Cancer Tissues by MALDI Imaging Mass Spectrometry. Journal of Proteome Research 9:1854–1863
24. Sanders ME, Dias EC, Xu BJ, Mobley JA, Billheimer D, Roder H, Grigorieva J, Dowsett M, Arteaga CL, Caprioli RM (2008) Differentiating Proteomic biomarkers in breast cancer by laser capture microdissection and MALDI MS. J Proteome Res 7:1500–1507

25. Hay ID, Thompson GB, Grant CS, Bergstralh EJ, Dvorak CE, Gorman CA, Maurer MS, McIver B, Mullan BP, Oberg AL et al (2002) Papillary thyroid carcinoma managed at the mayo clinic during six decades (1940–1999): temporal trends in initial therapy and long-term outcome in 2444 consecutively treated patients. World J Surg 26:879–885

26. Beasley NJP, Lee J, Eski S, Walfish P, Witterick I, Freeman JL (2002) Impact of nodal metastases on prognosis in patients with well-differentiated thyroid cancer. Arch Otolaryngol Head Neck Surg 128:825–828

27. Nucera C, Porrello A, Antonello ZA, Mekel M, Nehs MA, Giordano TJ, Gerald D, Benjamin LE, Priolo C, Puxeddu E et al (2010) B-RafV600E and thrombospondin-1 promote thyroid cancer progression. Proceedings of the National Academy of Sciences 107:10649–10654

28. Ricarte-Filho JC, Ryder M, Chitale DA, Rivera M, Heguy A, Ladanyi M, Janakiraman M, Solit D, Knauf JA, Tuttle RM et al (2009) Mutational Profile of Advanced Primary and Metastatic Radioactive Iodine-Refractory Thyroid Cancers Reveals Distinct Pathogenetic Roles for BRAF, PIK3CA, and AKT1. Cancer Research 69:4885–4893

29. Knauf JA, Sartor MA, Medvedovic M, Lundsmith E, Ryder M, Salzano M, Nikiforov YE, Giordano TJ, Ghossein RA, Fagin JA (2011) Progression of BRAF-induced thyroid cancer is associated with epithelial–mesenchymal transition requiring concomitant MAP kinase and TGF[beta] signaling. Oncogene 30:3153–3162

30. Vasko V, Espinosa AV, Scouten W, He H, Auer H, Liyanarachchi S, Larin A, Savchenko V, Francis GL, La Chapelle A et al (2007) Gene expression and functional evidence of epithelial-to-mesenchymal transition in papillary thyroid carcinoma invasion. Proceedings of the National Academy of Sciences 104:2803–2808

31. Stathatos N, Bourdeau I, Espinosa AV, Saji M, Vasko VV, Burman KD, Stratakis CA, Ringel MD (2005) KiSS-1/G protein-coupled receptor 54 metastasis suppressor pathway increases myocyte-enriched calcineurin interacting protein 1 expression and chronically inhibits calcineurin activity. J Clin Endocrinol Metab 90:5432–5440

32. Wreesmann VB, Sieczka EM, Socci ND, Hezel M, Belbin TJ, Childs G, Patel SG, Patel KN, Tallini G, Prystowsky M et al (2004) Genome-Wide Profiling of Papillary Thyroid Cancer Identifies MUC1 as an Independent Prognostic Marker. Cancer Research 64:3780–3789

33. Cerutti JM, Oler G, Michaluart P, Delcelo R, Beaty RM, Shoemaker J, Riggins GJ (2007) Molecular profiling of matched samples identifies biomarkers of papillary thyroid carcinoma lymph node metastasis. Cancer Res 67:7885–7892

34. Kim JW, Kim JH, Yoon SY, Joo JH, Lee Y, Lee KS, Chung JH, Choe S (2002) S100A6 protein as a marker for differential diagnosis of cholangiocarcinoma from hepatocellular carcinoma. Hepatol Res 23:274–286

35. Maelandsmo GM, Florenes VA, Mellingsaeter T, Hovig E, Kerbel RS, Fodstad O (1997) Differential expression patterns of S100A2, S100A4 and S100A6 during progression of human malignant melanoma. Int J Cancer 74:464–469

36. Ito Y, Yoshida H, Tomoda C, Uruno T, Miya A, Kobayashi K, Matsuzuka F, Kakudo K, Kuma K, Miyauchi A (2005) Expression of S100A2 and S100A6 in thyroid carcinomas. Histopathology 46:569–575

37. Brown LM, Helmke SM, Hunsucker SW, Netea-Maier RT, Chiang SA, Heinz DE, Shroyer KR, Duncan MW, Haugen BR (2006) Quantitative and qualitative differences in protein expression between papillary thyroid carcinoma and normal thyroid tissue. Mol Carcinog 45:613–626

38. Komatsu K, Kobune-Fujiwara Y, Andoh A, Ishiguro S, Hunai H, Suzuki N, Kameyama M, Murata K, Miyoshi J, Akedo H et al (2000) Increased expression of S100A6 at the invading fronts of the primary lesion and liver metastasis in patients with colorectal adenocarcinoma. Br J Cancer 83:769–774

39. Ohuchida K, Mizumoto K, Ishikawa N, Fujii K, Konomi H, Nagai E, Yamaguchi K, Tsuneyoshi M, Tanaka M (2005) The Role of S100A6 in Pancreatic Cancer Development and Its Clinical Implication as a Diagnostic Marker and Therapeutic Target. Clin Cancer Res 11:7785–7793

40. Vimalachandran D, Greenhalf W, Thompson C, Lüttges J, Prime W, Campbell F, Dodson A, Watson R, Crnogorac-Jurcevic T, Lemoine N et al (2005) High Nuclear S100A6 (Calcyclin) Is Significantly Associated with Poor Survival in Pancreatic Cancer Patients. Cancer Research 65:3218–3225

41. Breen EC, Tang K (2003) Calcyclin (S100A6) regulates pulmonary fibroblast proliferation, morphology, and cytoskeletal organization in vitro. J Cell Biochem 88:848–854

42. Sofiadis A, Dinets A, Orre LM, Branca RM, Juhlin CC, Foukakis T, Wallin G, Höög A, Hulchiy M, Zedenius J et al (2010) Proteomic Study of Thyroid Tumors Reveals Frequent Up-Regulation of the Ca2+−Binding Protein S100A6 in Papillary Thyroid Carcinoma. Thyroid 20:1067–1076

43. Kwon M, MacLeod TJ, Zhang Y, Waisman DM (2005) S100A10, annexin A2, and annexin a2 heterotetramer as candidate plasminogen. Front Biosci 10:300–325

44. Dano K, Behrendt N, Hoyer-Hansen G, Johnsen M, Lund LR, Ploug M, Romer J (2005) Plasminogen activation and cancer. Thromb Haemost 93:676–681

45. Nozaki S, Endo Y, Nakahara H, Yoshizawa K, Ohara T, Yamamoto E (2006) Targeting urokinase-type plasminogen activator and its receptor for cancer. Anticancer Drugs 17:1109–1117

46. Mochizuki M, Kwon Y-W, Yodoi J, Masutani H (2009) Thioredoxin regulates cell cycle via the ERK1/2-cyclin D1 pathway. Antioxid Redox Signal 11:2957–2971

47. Powis G, Kirkpatrick DL (2007) Thioredoxin signaling as a target for cancer therapy. Curr Opin Pharmacol 7:392–397

48. Akhurst RJ, Derynck R (2001) TGF-beta signaling in cancer—a double-edged sword. Trends Cell Biol 11:44–51

49. Massagué J, Blain SW, Lo RS (2000) TGF[beta] signaling in growth control, cancer, and heritable disorders. Cell 103:295–309

50. Elliott RL, Blobe GC (2005) Role of transforming growth factor beta in human cancer. J Clin Oncol 23:2078–2093

51. Bierie B, Moses HL (2006) Tumour microenvironment: TGF [beta]: the molecular Jekyll and Hyde of cancer. Nat Rev Cancer 6:506–520

52. Laverty HG, Wakefield LM, Occleston NL, O'Kane S, Ferguson MWJ (2009) TGF-[beta]3 and cancer: A review. Cytokine Growth Factor Rev 20:305–317

53. Feighery R, Maguire P, Ryan MP, McMorrow T (2008) A proteomic approach to immune-mediated epithelial-mesenchymal transition. Proteomics Clin Appl 2:1110–1117

54. Grande M, Franzen A, Karlsson J-O, Ericson LE, Heldin N-E, Nilsson M (2002) Transforming growth factor-{beta} and epidermal growth factor synergistically stimulate epithelial to mesenchymal transition (EMT) through a MEK-dependent mechanism in primary cultured pig thyrocytes. J Cell Sci 115:4227–4236

55. Rr I, Db R (1983) Plasminogen is present in the basal layer of the epidermis. J Investig Dermatol 80:297–299

56. Andreasen PA, Egelund R, Petersen HH (2000) The plasminogen activation system in tumor growth, invasion, and metastasis. Cell Mol Life Sci 57:25–40